PCCP

An *ab initio* direct classical trajectory study of s-tetrazine photodissociation

Xiaosong Li, Smriti Anand, John M. Millam† and H. Bernhard Schlegel*

Department of Chemistry, Wayne State University, Detroit, MI 48202, USA

Received 17th December 2001, Accepted 11th March 2002
First published as an Advance Article on the web 9th May 2002

The photodissociation of s-tetrazine *via* a three-body fragmentation channel ($C_2N_2H_2 \rightarrow 2HCN + N_2$) has been studied by *ab initio* direct classical trajectory calculations using Hartree–Fock and density functional methods with split valence and polarized basis sets [HF/3-21G, HF/6-31G(d) and B3LYP/6-31G(d)]. The calculated transition state is planar. At our most reliable method (CBS-APNO), the heat of reaction and barrier height are -53.0 kcal mol^{-1} and 41.1 kcal mol^{-1}, respectively. To simulate the experimental photolysis of s-tetrazine, trajectories were started from a microcanonical ensemble at the transition state with 12 kcal mol^{-1} excess energy distributed among the vibrational modes and the transition vector. At all levels of theory, the HCN product has a very broad rotational distribution, ranging up to $J = 64$, and has extensive excitation of the bending vibration. By contrast, N_2 is produced with low J and with only a small amount of vibrational excitation in agreement with experiments. In accord with the experiment, the relative translation motion of the products receives about 80–83% of the available energy.

Introduction

The photochemical decomposition of s-tetrazine has been of interest to both the experimental and theoretical communities[1–11] since the 1975 experiment by Hochstrasser and King,[1] which suggested that the electronically excited s-tetrazine undergoes nonradiative decay and fragmentation producing molecular nitrogen and hydrogen cyanide. In 1977, Hochstrasser *et al.* proposed several plausible mechanisms (eqn. (1)–(3)) for the photodissociation process.[3]

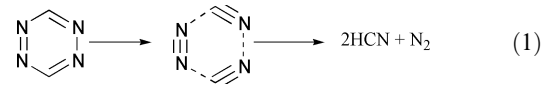

(1)

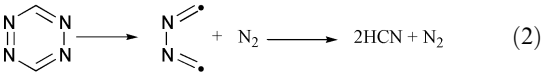

(2)

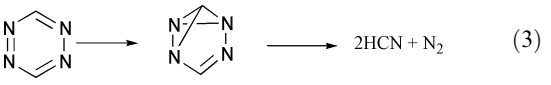

(3)

Among these possible pathways, the most intriguing one is the concerted fragmentation [channel (1)], since it is rare that unimolecular dissociation involves one transition state and three fragments. Subsequent theoretical studies by Schaefer and Scuseria indicated that channel (1) is orbital symmetry allowed and energetically operative under the conditions of the experiments.[4,6,10] By using configuration interaction and coupled cluster methods, Schaefer and Scuseria predicted a planar transition state with a barrier height of 33.1–38.1 kcal mol^{-1}, which is in agreement with the activation energy of 39.7 kcal mol^{-1} obtained from the thermal decomposition experiment by Windisch, Smith and Hochstrasser,[7] and is less than the photoexcitation ($S_0 \rightarrow S_1$) threshold of 51.8 kcal mol^{-1}.[8] In 1989, Zhao, Miller, Hintsa and Lee presented time-of-flight spectra, which suggested that s-tetrazine underwent a concerted triple dissociation.[5] Furthermore, the same authors reported that the average translational energy of the products is 82.2 kcal mol^{-1} for excitation at 18830.9 cm^{-1} and that there is a stronger repulsion between the two HCN fragments than between HCN and N_2. Nahon and co-workers reported the detailed vibrational energy content of the fragments by photoelectron spectroscopy.[9] Their results are also consistent with a pure three body fragmentation mechanism, and they found about 5.4% of nitrogen and 26% of each HCN fragments are vibrationally excited. It is now generally recognized that, similar to glyoxal (for leading references, see ref. 12), the photoexcitation of s-tetrazine from S_0 to S_1 state is followed by a rapid internal conversion to the highly vibrationally excited manifold of the ground state potential energy surface. Both theoretical and experimental work supports the concerted unimolecular three-body fragmentation of s-tetrazine *via* channel (1).[1–11]

Because of advances in computer speed and improvements in molecular orbital software, it has become possible to compute classical trajectories directly from electronic structure calculations without first fitting a global potential energy surface.[13] Whenever energies, gradients or Hessians are needed for the trajectory integration, they are computed "on the fly" by molecular orbital methods. Similar to our studies of glyoxal and formaldehyde photodissociation,[14–18] we have used *ab initio* trajectory calculations to investigate the dynamics of the s-tetrazine three-body dissociation.

Method

The development version of the GAUSSIAN series of programs was used to carry out all computations in the present study.[19] The geometries of ground state s-tetrazine and its transition state were optimized at the following levels of theory: Hartree–Fock [HF/3-21G, HF/6-31G(d), HF/6-31G(d)], second order Møller–Plesset perturbation theory [MP2/6-31G(d)], Becke's three parameter hybrid functional method[20] [B3LYP/6-31G(d)], a modified version of Becke's half-and-

† Semichem, P. O. Box 1649, Shawnee Mission, KS 66222, USA.

 DOI: 10.1039/b111390a

half density functional method[21] [BH&HLYP/6-311G(d,p)] and quadratic configuration interaction with single and double excitations[22] [QCISD/6-311G(d,p)]. The complete basis set extrapolation method of Petersson and co-workers with the atomic pair natural orbital basis set (CBS-APNO)[23] was used to compute accurate heats of reaction and enthalpies of activation. The mass-weighted steepest descent reaction paths were calculated using the method of Gonzalez and Schlegel.[24,25]

Ab-initio classical trajectories were integrated using the Hessian based predictor-corrector method.[26,27] The Hessian was updated for five steps before being recalculated analytically. The step-size used for all the calculations was 0.5 $u^{1/2}$ a_0. The trajectories were terminated when the products were at least 8 a_0 apart and the gradient of the potential between the products was less than 1×10^{-5} E_h a_0^{-1}. The average time taken for a trajectory to complete was about 100 fs and the total energy was conserved to about 10^{-7} E_h.

The initial conditions for the trajectory calculations were chosen to simulate the experimental photolysis of s-tetrazine from the zero point level of the S_1 state, which corresponds to 51.8 kcal mol^{-1} energy above the s-tetrazine ground state or 12 kcal mol^{-1} above the transition state for triple dissociation. The trajectories were started at the transition state on S_0 and a microcanonical ensemble was constructed using quasiclassical normal mode sampling,[28] distributing $E_{tot} = 12$ kcal mol^{-1} excess energy among the 17 vibrational normal modes and translation along the transition vector. The total angular momentum was set to zero since the reactant is rotationally cold under experimental conditions. All the possible vibrational states up to 12 kcal mol^{-1} were generated within the harmonic oscillator approximation. For the motion along the reaction coordinate (*i.e.* along the transition vector), a uniform distribution of momentum in the direction of the products was used. For a given translational energy along the transition vector, E_{trn}, all vibrational states between $E_{tot} - E_{trn} - \Delta E/2$ and $E_{tot} - E_{trn} + \Delta E/2$ were selected; ΔE was adjusted to yield the desired number of states. For a specific vibrational mode with a given number of quanta, the initial phase was chosen randomly. Since the actual potential energy surface is not strictly harmonic, the initial vibrational coordinates and momenta generated by this procedure were scaled to yield the desired vibrational energy.[28] Approximately 200 trajectories were integrated at the HF/3-21G, HF/6-31G(d) and B3LYP/6-31G(d) levels of theory. A detailed list of the initial states for the HF/3-21G, HF/6-31G(d) and B3LYP/6-31G(d) trajectories is available at http://www.chem.wayne.edu/Schlegel/supp-mat/. Error bars of one standard deviation were included in the appropriate plots.

For the product rotational distribution, the instantaneous angular velocity is given by

$$\omega = \sum_i \boldsymbol{r}_i \times \dot{\boldsymbol{r}}_i$$

where $\boldsymbol{r}_i$ is the ith position vector. To analyze the vibrational energy of the N_2 product, a Morse function was fit to the potential energies at several distances. The Morse function was used to obtain the vibrational quantum numbers of the diatomic product by integrating the momentum over one vibration period using the Einstein–Brillouin–Keller (EBK) semiclassical quantization condition.[29,30] For the polyatomic product, the vibrational kinetic energy for each mode was obtained by decomposing the mass-weighted velocity into the instantaneous normal modes.[31] The vibrational potential energy for each mode was estimated by assuming a local harmonic approximation:

$$E_{pot,i} = g_i^2 H_{ii}^{-1}/2$$

where g_i is the gradient and H_{ii} is the Hessian element for the ith instantaneous normal mode. However, this equation is not accurate enough to analyze HCN vibrations since the potential is rather anharmonic. Comparison of calculated harmonic frequencies and observed anharmonic frequencies[32] suggests that a single scale factor can be used as a good first approximation to correct for the anharmonicity in all of the vibrational modes.[33] Based on this observation, we estimate a uniform scale factor for all the normal modes of the HCN product to correct for the anharmonicity of the potential as we distort HCN from the following equation:

$$f = \frac{\sum_i E_{pot,i}}{E_{act}}$$

where $E_{pot,i}$ is the predicted harmonic potential energy for the displacement along the ith normal mode and E_{act} is the actual potential energy difference for distorting the HCN fragment calculated directly from the electronic structure theory. The potential energy of each of the normal modes was scaled by this factor (note that the scale factor will be different for each different distortion of the HCN products). The vibrational quantum numbers are obtained from the kinetic and scaled potential energies for each normal mode.

Results and discussion

Structures and energetics

The calculated and experimental geometric parameters for the ground state of s-tetrazine are collected in Table 1. At HF/3-21G, B3LYP/6-31G(d) and all the post-SCF levels of theory considered, the calculations agree well with experiment[34] and with previous calculations.[6] However, at HF/6-31G(d), CN and NN bond lengths are about 0.03 Å too short. The calculated geometric parameters for the transition state of s-tetrazine are listed in Table 2. The B3LYP geometry agrees well with the QCISD and CCSD calculations, but the N_1–N_2, N_3–N_4 and C_2–N_4 bonds are too short in the HF structures. In agreement with the calculations by Schaefer and Scuseria,[6] the theoretical geometry for the transition state for the concerted unimolecular triple dissociation of s-tetrazine is planar. At the transition state, the bond length for the departing N_2 is 1.172 Å at QCISD/6-311G(d,p), 70% of the way from the N–N bond length in s-tetrazine to the N_2 equilibrium geometry. However, the change in the HCN bond angle is only 22% complete in the transition state. Since the HCN group in the transition geometry is still far from its linear equilibrium structure, the bending mode of the hydrogen cyanide will probably be excited in the product. The calculated vibrational frequencies are listed in Table 3. For the equilibrium geometry of s-tetrazine, these are in good agreement with the available experimental data. All of the optimized transition states are first order saddle points. However, the imaginary frequency at the B3LYP level is significantly smaller than at HF or MP2.

Table 4 summarizes the calculated barrier heights and heats of reaction. The heats of reaction predicted at the Hartree–Fock level of theory are about 17–27 kcal mol^{-1} more exothermic than our most accurate value of -53.0 kcal mol^{-1} at CBS-APNO level of theory. All the CBS methods predict the reaction heats within 2 kcal mol^{-1} of the experimental estimate of -51 kcal mol^{-1} reported in 1978 by Coulter and coworkers.[35] Except for HF/6-31G(d) and BH&HLYP/6-31G(d), all the levels of theory predict the barrier heights within ± 7 kcal mol^{-1} of the experimental activation energy of 39.7 kcal mol^{-1} for the thermal decomposition.[7] However, the energy released in going from the transition state to the products is 35–50 kcal mol^{-1} too high at the HF level, and 10–15 kcal mol^{-1} too low at B3LYP. As expected, the G2 and CBS methods are in quite good agreement with the experimental estimates.

For reaction (2), a lower bound for the heat of reaction can be computed using the triplet state of the HCNNCH diradical. At the CBS-APNO level, this intermediate lies 86.4 kcal mol^{-1}

Table 1 Optimized geometries for the ground state of s-tetrazine[a]

	C–N	C–H	N–N	∠NCH
HF/3-21G	1.329	1.064	1.331	117.6
HF/6-31G(d)	1.318	1.071	1.291	117.4
B3LYP/6-31G(d)	1.339	1.086	1.326	116.7
MP2/6-31G(d)	1.345	1.086	1.340	116.4
QCISD/6-311G(d, p)	1.340	1.084	1.322	116.7
CCSD/DZP[b]	1.346	1.087	1.331	116.6
Experiment[c]	1.341	1.073	1.326	116.8

[a] Bond lengths in Å, angles in degrees. [b] Ref. 6. [c] Ref. 34.

Table 2 Optimized geometries for the transition state of s-tetrazine[a]

	N_1–N_2	C_2–H_2	C_2–N_4	N_3–N_4	C_2–N_2	∠$H_2C_2N_4$	∠$N_2C_2H_2$
HF/3-21G	1.155	1.060	1.195	1.850	1.762	133.3	101.9
HF/6-31G(d)	1.138	1.066	1.186	1.869	1.768	132.6	102.3
B3LYP/6-31G(d)	1.170	1.079	1.211	1.930	1.754	131.2	103.4
MP2/6-31G(d)	1.200	1.082	1.234	1.841	1.679	126.8	106.0
QCISD/6-311G(d, p)	1.172	1.079	1.216	1.902	1.744	130.5	103.7
CCSD/DZP[b]	1.183	1.083	1.224	1.926	1.759	130.9	103.3

[a] Bond lengths in Å, angles in degrees; see Fig. 1 for atom numbering. [b] Ref. 6.

Table 3 Vibrational frequencies for s-tetrazine ground state and transition state[a]

	ν_1	ν_2	ν_3	ν_4	ν_5	ν_6	ν_7	ν_8	ν_9	ν_{10}	ν_{11}	ν_{12}	ν_{13}	ν_{14}	ν_{15}	ν_{16}	ν_{17}	ν_{18}
Ground state																		
HF/3-21G	391	407	626	636	748	818	975	984	1033	1044	1073	1186	1308	1397	1421	1495	3120	3139
HF/6-31G(d)	367	404	632	738	791	804	926	987	1053	1066	1140	1235	1297	1474	1550	1603	3084	3086
B3LYP/6-31G(d)	246	328	622	728	790	890	950	955	1009	1053	1113	1189	1283	1425	1429	1510	3106	3107
MP2/6-31G(d)	250	318	603	706	753	869	924	956	1018	1043	1155	1160	1266	1359	1399	1470	3088	3089
Experiment[b]	254	255	640	736	801	882	904	994	1009	–	1103	1200	1291	1415	1435	1525	3010	3090
Transition state																		
HF/3-21G	1010i	161	161	393	396	469	611	667	712	852	883	1038	1093	1505	1869	1887	3183	3183
HF/6-31G(d)	1114i	134	147	335	362	432	585	630	690	804	836	999	1037	1547	1906	2013	3144	3144
B3LYP/6-31G(d)	629i	93	144	301	347	451	556	611	726	762	793	1029	1068	1609	1839	1910	3174	3174
MP2/6-31G(d)	972i	80	143	318	375	504	581	625	747	777	838	1039	1133	1385	1710	1718	3130	3131

[a] Harmonic frequencies in cm^{-1}; scale factors 0.9085 for HF/3-21G, 0.8953 for HF/6-31G(d), 0.9434 for B3LYP/6-31G(d), 0.9614 for MP2/6-31G(d).[32] [b] Refs. 37–40.

above s-tetrazine. Since only 51.8 kcal mol^{-1} is available from photoexcitation at the $S_0 \rightarrow S_1$ threshold, reaction (2) cannot contribute to the dissociation of s-tetrazine under these conditions.

Reaction path

Fig. 2 shows the potential energy profile along the mass-weighted steepest descent reaction path (intrinsic reaction coordinate). The B3LYP potential energy profile is much broader than for HF or MP2, in keeping with the significantly smaller imaginary frequency computed at the transition state (see Table 3). For dissociation, the broader profile corresponds to greater repulsion between products at a given separation. Most of the geometry change in the N_2 bond length is finished by $s = 1.5\ u^{1/2}\ a_0$ [this corresponds to N–N bond length of 1.091 Å at HF/3-21G, 1.083 Å at HF/6-31G(d) level and 1.126 Å at B3LYP/6-31G(d)]. Only about 15–22% of energy has been released by this point, compared to 50% for formaldehyde at $s = 1\ u^{1/2}\ a_0$.[15] This is understandable since, as in glyoxal, there is more van der Waals repulsion between the 3 fragments in the reaction than between the 2 fragments in formaldehyde dissociation. At this point, the HCN bond angle is 148.2°, suggesting the bending mode of HCN will be vibrationally excited.

Dynamics

Fig. 3 compares the rotational populations of HCN and N_2 obtained from trajectories computed at the HF/3-21G, HF/6-31G(d) and B3LYP/6-31G(d) levels. At the two HF levels of theory, the rotational distributions are similar. It can be seen that HCN has a much broader rotational distribution than N_2, ranging up to $J = 64$ at the HF/6-31G(d) level. The calculated average rotational quantum numbers are 29–31 for the HCN and 6–7 for the N_2 at the HF level, which are equivalent to energies of 6.4–6.9 kcal mol^{-1} and ~0.3 kcal mol^{-1}, respectively. However, calculations at B3LYP/6-31G(d) show quite different rotational distributions for both N_2 and HCN fragments, as a result of the greater repulsion between the products as they dissociate. N_2 is produced with much higher rotational quantum numbers, ranging up to $J = 27$. HCN has a somewhat narrower distribution than those at HF level. The calculated average rotational quantum numbers at B3LYP are 24 and 16 for HCN and N_2, respectively, corresponding to energies of 3.5 and 1.5 kcal mol^{-1}.

Table 4 Reaction enthalpies and barrier heights for s-tetrazine[a]

	$\Delta H^{\circ}_{r,298}$	$\Delta H^{\ddagger}_{298,forward}$	$\Delta H^{\ddagger}_{298,backward}$
HF/3-21G	−80.3	46.2	126.5
HF/6-31G(d)	−70.0	71.3	141.3
BH&HLYP/6-31G(d)	−38.8	58.4	97.2
B3LYP/6-31G(d)	−37.0	43.3	80.3
MP2/6-31G(d)	−62.7	40.9	103.6
G2	−54.3	39.0	93.3
CBS-Q	−51.0	39.7	90.7
CBS-QB3	−51.2	42.6	93.8
CBS-APNO	−53.0	41.1	94.1
Experiment	−51[b]	39.7[c]	90.7

[a] Enthalpies at 298 K in kcal mol^{-1}. [b] Ref. 35. [c] Ref. 7.

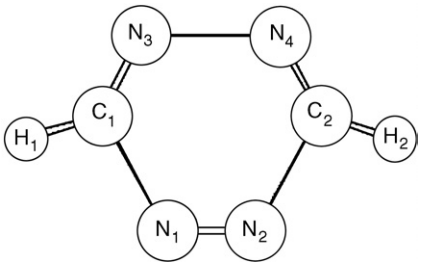

Fig. 1 Optimized geometry of the transition state for s-tetrazine → N_2 + 2HCN.

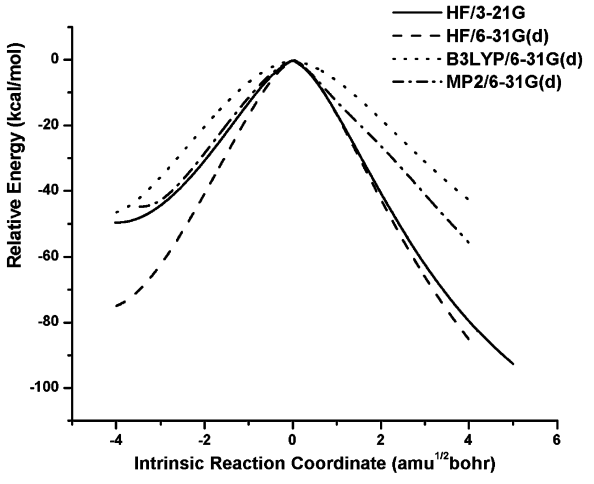

Fig. 2 Potential energy along the reaction path for s-tetrazine → N_2 + 2HCN at HF/3-21G, HF/6-31G(d), B3LYP/6-31G(d), and MP2/6-31G(d).

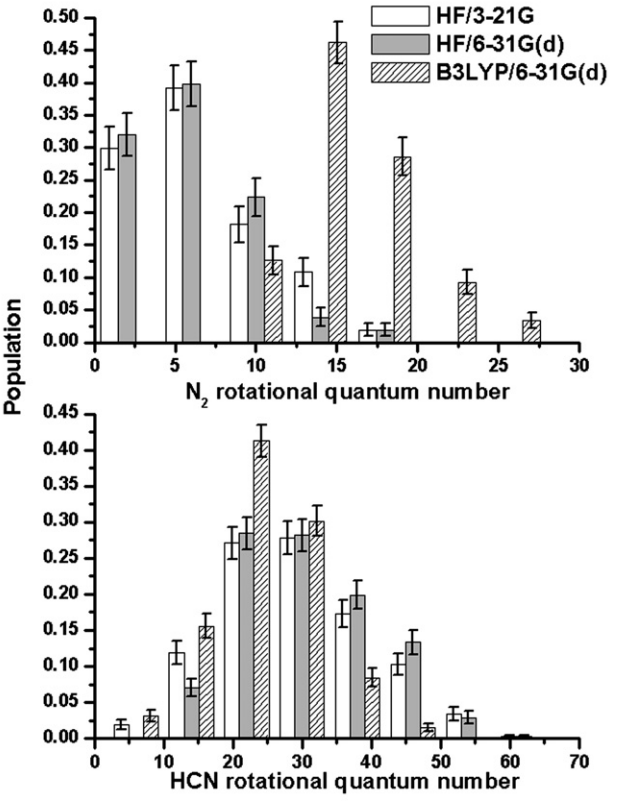

Fig. 3 Rotational populations for HCN and N_2 at HF/3-21G, HF/6-31G(d) and B3LYP/6-31G(d) for a microcanonical ensemble with 12 kcal mol^{-1} excess energy.

Calculations show a small amount of vibrational excitation for the N_2 product at the HF level (Table 5), which is in agreement with the experimental result. N_2 produced at B3LYP/6-31G(d) has no vibrational excitation. As might be anticipated from the transition state geometry and the reaction path calculations, the HCN fragment has a significant vibrational excitation in its bending modes. The anharmonic corrections described in the Method section are applied to each of the normal modes, and the resulting vibrational distributions for the three normal modes of the HCN products are listed in Table 6. Compared to the observed vibrational distribution for HCN bending (70% in $v = 0$ and 26% in $v = 1$ to $v = 6$),[9] the calculations show too much vibrational excitation in this mode. The HF level of theory predicts about 32–47 kcal mol^{-1} too much energy released along the reaction path than experiment, and B3LYP predicts 14 kcal mol^{-1} too little energy release. Thus, the apparent excess energy in the HCN vibrations cannot be explained by errors in the calculated energy release. Analysis of the calculated vibrational energy in terms of the equilibrium normal modes instead of the instantaneous normal modes and a more elaborate correction for anharmonicity may impose the agreement with experiment.

The average product translational energies are summarized in Table 7. Of the available energy (the energy released plus 12 kcal mol^{-1} excess energy above the transition state), 20–22% goes to N_2 and 60–61% to HCN translation. The total percentage of 80–83% compares well with 77% obtained by Zhao *et al.* on the basis of photofragment translational spectroscopy measurements.[5] The latter has been recalculated using 82.2 kcal mol^{-1} experimental translational energy,[5] 53.8 kcal mol^{-1} photon energy for excitation to $6a_0^1$ of S_1,[5] and −53.0 kcal mol^{-1} heat of reaction (CBS-APNO calculation in this work).

Table 5 Vibrational distributions for the N_2 fragment

	Frequency/cm^{-1} [a]	$v = 0$	$v = 1$	$v = 2$
HF/3-21G	2373.5	97.1	2.4	0.5
HF/6-31G(d)	2469.2	98.1	1.9	
B3LYP/6-31G(d)	2309.0	100.0		
Experiment	2359.6[b]	94.6 ± 0.5[c]	5.4 ± 0.5[c]	

[a] Harmonic frequencies in cm^{-1}; for scale factors, see Table 3. [b] Ref. 36. [c] Ref. 9.

Table 6 Vibrational distributions for the HCN fragment

	Frequency/cm^{-1} [a]	$v = 0$	$v = 1$	$v = 2$	$v = 3$	$v = 4$
HF/3-21G						
Bending	899.1	56.9	34.0	6.8	1.8	0.5
CN stretching	2175.5	56.1	34.0	7.9	1.8	0.2
CH stretching	3353.5	89.5	10.5			
HF/6-31G(d)						
Bending	797.3	48.1	38.4	10.5	2.7	0.3
CN stretching	2183.6	51.7	46.4	1.9		
CH stretching	3292.6	85.6	13.9	0.5		
B3LYP/6-31G(d)						
Bending	723.3	48.5	28.3	15.6	6.3	0.8
CN stretching	2088.1	64.6	21.9	6.8	2.5	
CH stretching	3283.7	100.0				

[a] Harmonic frequencies in cm^{-1}; for scale factors, see Table 3.

Table 7 Average partitioning of available energy into translation

Product	Method	Energy/kcal mol^{-1}	% Energy disposal
N_2	HF/3-21G	28.0	19.6
	HF/6-31G(d)	35.2	22.8
	B3LYP/6-31G(d)	17.3	19.6
2 HCN	HF/3-21G	87.2	61.1
	HF/6-31G7(d)	92.6	59.9
	B3LYP/6-31G(d)	53.4	60.4
Total	HF/3-21G	105.2	80.7
	HF/6-31G(d)	127.8	82.7
	B3LYP/6-31G(d)	70.7	79.8

Conclusion

Direct classical trajectories for s-tetrazine three-body fragmentation were calculated at the HF/3-21G, HF/6-31G(d) and B3LYP/6-31G(d) levels of theory. The computed rotational distribution for HCN is broad with $\langle J \rangle = 24$–31. In qualitative agreement with experiment, the calculations produce HCN with a high degree of excitation in the bending mode. However, the calculations yield much higher populations in the excited modes than seen experimentally. The HF and B3LYP potential energy surfaces differ significantly in shape and energy released, yet HF/3-21G, HF/6-31G(d) and B3LYP/6-31G(d) trajectories all yield more vibrational excitation of HCN than observed experimentally. There may be causes other than the level of theory that could account for the difference between the calculated and observed degree of vibrational excitations. One possibility is that the internal conversion from S_1 to S_0 yields an initial distribution that does not correspond to a rotationally cold microcanonical ensemble at the transition state. Alternatively, the vibrational energy distribution may have relaxed in the *ca.* 100 ns between the photolysis and the measurement of the vibrational populations of the products. The N_2 is produced with low J and with very little vibrational excitation, which is in good agreement with the experiments. The total translation receives about 80% of the available energy, which is in accord with the experiment.

Acknowledgement

This work was supported by grant from the National Science Foundation (CHE 9874005 and CISE 9977815). The authors would like to thank William L. Hase for helpful discussions, and Wayne State University for computer time.

References

1 R. M. Hochstrasser and D. S. King, *J. Am. Chem. Soc.*, 1975, **97**, 4760.
2 R. M. Hochstrasser, D. S. King and A. B. Smith, *J. Am. Chem. Soc.*, 1977, **99**, 3923.
3 D. S. King, C. T. Denny, R. M. Hochstrasser and A. B. Smith, *J. Am. Chem. Soc.*, 1977, **99**, 271.
4 A. C. Scheiner, G. E. Scuseria and H. F. Schaefer III, *J. Am. Chem. Soc.*, 1986, **108**, 8160.

5 X. S. Zhao, W. B. Miller, E. J. Hintsa and Y. T. Lee, *J. Chem. Phys.*, 1989, **90**, 5527.
6 G. E. Scuseria and H. F. Schaefer III, *J. Phys. Chem.*, 1990, **94**, 5552.
7 V. L. Windisch, A. B. Smith and R. M. Hochstrasser, *J. Phys. Chem.*, 1988, **92**, 5366.
8 C. A. Haynam, D. V. Brumbaugh and D. H. Levy, *J. Chem. Phys.*, 1984, **81**, 2270.
9 L. Nahon, P. Morin, M. Larzilliere and I. Nenner, *J. Chem. Phys.*, 1992, **96**, 3628.
10 A. C. Scheiner and H. F. Schaefer III, *J. Chem. Phys.*, 1987, **87**, 3539.
11 A. C. Scheiner, G. E. Scuseria and H. F. Schaefer III, *J. Am. Chem. Soc.*, 1986, **108**, 8160.
12 L. M. Dobeck, H. M. Lambert, W. Kong, P. J. Pisano and P. L. Houston, *J. Phys. Chem. A*, 1999, **103**, 10 312.
13 K. Bolton, W. L. Hase, G. H. Peslherbe, in *Modern Methods for Multidimensional Dynamics Computation in Chemistry*, ed. D. L. Thompson, World Scientific, Singapore, 1998, p. 143.
14 W. Chen, W. L. Hase and H. B. Schlegel, *Chem. Phys. Lett.*, 1994, **228**, 436.
15 X. Li, J. M. Millam and H. B. Schlegel, *J. Chem. Phys.*, **113**, 10 062.
16 X. Li, J. M. Millam and H. B. Schlegel, *J. Chem. Phys.*, 2001, **114**, 8897.
17 X. Li, J. M. Millam and H. B. Schlegel, *J. Chem. Phys.*, 2001, **115**, 6907.
18 X. S. Li and H. B. Schlegel, *J. Chem. Phys.*, 2001, **114**, 8.
19 M. J. Frisch, G. W. Trucks, H. B. Schlegel, G. E. Scuseria, M. A. Robb, J. R. Cheeseman, V. G. Zakrzewski, J. A. Montgomery, R. E. Stratmann, J. C. Burant, S. Dapprich, J. M. Millam, A. D. Daniels, K. N. Kudin, M. C. Strain, O. Farkas, J. Tomasi, V. Barone, M. Cossi, R. Cammi, B. Mennucci, C. Pomelli, C. Adamo, S. Clifford, J. Ochterski, G. A. Petersson, P. Y. Ayala, Q. Cui, K. Morokuma, D. K. Malick, A. D. Rabuck, K. Raghavachari, J. B. Foresman, J. Cioslowski, J. V. Ortiz, B. B. Stefanov, G. Liu, A. Liashenko, P. Piskorz, I. Komaromi, R. Gomperts, R. L. Martin, D. J. Fox, T. Keith, M. A. Al-Laham, C. Y. Peng, A. Nanayakkara, C. Gonzalez, M. Challacombe, P. M. W. Gill, B. G. Johnson, W. Chen, M. W. Wong, J. L. Andres, M. Head-Gordon, E. S. Replogle, J. A. Pople, *Gaussian 98*, Gaussian, Inc., Pittsburgh, PA.
20 A. D. Becke, *J. Chem. Phys.*, 1993, **98**, 5648.
21 A. D. Becke, *J. Chem. Phys.*, 1993, **98**, 1372.
22 J. A. Pople, M. Head-Gordon and K. Raghavachari, *J. Chem. Phys.*, 1987, **87**, 5968.
23 J. A. Montgomery, J. W. Ochterski and G. A. Petersson, *J. Chem. Phys.*, 1994, **101**, 5900.
24 C. Gonzalez and H. B. Schlegel, *J. Chem. Phys.*, 1989, **90**, 2154.
25 C. Gonzalez and H. B. Schlegel, *J. Phys. Chem.*, 1990, **94**, 5523.
26 J. M. Millam, V. Bakken, W. Chen, W. L. Hase and H. B. Schlegel, *J. Chem. Phys.*, 1999, **111**, 3800.
27 V. Bakken, J. M. Millam and H. B. Schlegel, *J. Chem. Phys.*, 1999, **111**, 8773.
28 W. L. Hase, in *Encyclopedia of Computational Chemistry*, ed. P. v. R. Schleyer, N. L. Allinger, T. Clark, J. Gasteiger, P. A. Kollman, H. F. Schaefer III and P. R. Schreiner, Wiley, New York, 1998, p. 402.
29 M. C. Gutzwiller, *Chaos in Classical and Quantum Mechanics*, Springer-Verlag, New York, 1990.
30 W. L. Hase, in *Encyclopedia of Computational Chemistry*, ed. P. v. R. Schleyer, N. L. Allinger, T. Clark, J. Gasteiger, P. A. Kollman, H. F. Schaefer III and P. R. Schreiner, Wiley, New York, 1998, p. 399.
31 L. M. Raff, *J. Chem. Phys.*, 1988, **89**, 5680.
32 A. P. Scott and L. Radom, *J. Phys. Chem.*, 1996, **100**, 16 502.
33 Y. M. Rhee and M. S. Kim, *J. Chem. Phys.*, 1997, **107**, 1394.
34 V. A. Job and K. K. Innes, *J. Mol. Spectrosc.*, 1978, **71**, 299.
35 D. Coulter, D. Dows, H. Reisler and C. Wittig, *Chem. Phys.*, 1978, **32**, 429.
36 G. Herzberg, *Molecular Spectra and Molecular Structure I, Spectra of Diatomic Molecules*, Van Nostrand, New York, 1950.
37 L. A. Franks, A. J. Merer and K. K. Innes, *J. Mol. Spectrosc.*, 1968, **26**, 458.
38 D. V. Brumbaugh and K. K. Innes, *Chem. Phys.*, 1981, **59**, 413.
39 K. B. Thakur, V. A. Job and V. B. Kartha, *J. Mol. Spectrosc.*, 1984, **107**, 373.
40 K. B. Thakur, V. A. Job and V. B. Kartha, *J. Mol. Spectrosc.*, 1985, **112**, 340.